The Red Blood Cell Glucose Transporter Presents Multiple, Nucleotide-Sensitive Sugar Exit Sites†

Erin K. Cloherty, Kara B. Levine, and Anthony Carruthers*

Department of Biochemistry and Molecular Pharmacology, University of Massachusetts Medical School, 55 Lake Avenue North, Worcester, Massachusetts 01655

Received July 18, 2001; Revised Manuscript Received October 5, 2001

ABSTRACT: At any instant, the human erythrocyte sugar transporter presents at least one sugar export site but multiple sugar import sites. The present study asks whether the transporter also presents more than one sugar exit site. We approached this question by analysis of binding of [^{3}H]cytochalasin B (an export conformer ligand) to the human erythrocyte sugar transporter and by analysis of cytochalasin B modulation of human red blood cell sugar uptake. Phloretin-inhibitable cytochalasin B binding to human red blood cells, to human red blood cell integral membrane proteins, and to purified human red blood cell glucose transport protein (GluT1) displays positive cooperativity at very low cytochalasin B levels. Cooperativity between sites and $K_{d(app)}$ for cytochalasin B binding are reduced in the presence of intracellular ATP. Red cell sugar uptake at subsaturating sugar levels is inhibited by high concentrations of cytochalasin B but is stimulated by lower (<20 nM) concentrations. Increasing concentrations of the e1 ligand forskolin also first stimulate then inhibit sugar uptake. Cytochalasin D (a cytochalasin B analogue that does not interact with GluT1) is without effect on sugar transport over the same concentration range. Cytochalasin B and ATP binding are synergistic. ATP (but not AMP) enhances [^{3}H]cytochalasin B photoincorporation into GluT1 while cytochalasin B (but not cytochalasin D) enhances [γ-^{32}P]azidoATP photoincorporation into GluT1. We propose that the red blood cell glucose transporter is a cooperative tetramer of GluT1 proteins in which each protein presents a translocation pathway that alternates between uptake (e2) and export (e1) states but where, at any instant, two subunits must present uptake (e2) and two subunits must present exit (e1) states.

Protein-mediated solute transport across cell membranes proceeds via membrane-spanning channels and carriers. For most carrier-mediated transfer systems, the mechanism of solute transport is consistent with a ping-pong transfer process. Here, the carrier alternates between one state ("e1") presenting a substrate export site and a second state ("e2") exposing a substrate import site (*1*, *2*). Solute translocation occurs when the carrier−substrate complex undergoes the e1 → e2 or e2 → e1 transition.

The human red blood cell glucose transporter is one of several carrier-mediated transport systems that do not function in this manner (*3*−*7*). Instead, the erythrocyte sugar transporter presents sugar uptake and sugar efflux sites simultaneously (*8*−*11*). This behavior seems not to result from the internal duplication of a catalytic domain because most carrier proteins—those functioning as ping-pong carriers and those that function as simultaneous carriers—present a fundamentally similar secondary structure of 10−14 membrane spanning domains (*12*−*15*). How can transport systems that share a common secondary structure and, in some instances, homologous primary structure display fundamental differences in catalytic behavior?

We have proposed (*11*) that the human erythrocyte glucose transporter is a GluT1[1] homotetramer and that each GluT1 protein (transporter subunit) provides a sugar translocation pathway acting as a ping-pong carrier. Although each subunit presents the same membrane topology/orientation, cooperative interactions between subunits are hypothesized to result in a nonrandom arrangement of catalytic states within the transport complex. At any given instant, two subunits must exist in the e1 state and two subunits must be present the e2 state. If one GluT1 protein undergoes the e1 → e2 transition, its neighbor must undergo the reverse or e2 → e1 transition and vice versa. In this manner, the glucose transporter complex, although comprised of individual ping-pong carriers, behaves as a simultaneous carrier presenting uptake and efflux sites to sugars concurrently.

Biochemical, biophysical, and molecular biological studies of GluT1 quaternary structure and kinetic behavior (transport and ligand binding) have resulted in contrary interpretations

† This work was supported by NIH Grants DK 44888 and DK 36081.

* To whom correspondence should be addressed. E-mail: anthony.carruthers@umassmed.edu. Telephone: 508-856-5570. Fax: 508-856-6231.

[1] Abbreviations: GluT1, human erythrocyte glucose transport protein; 3MG, 3-*O*-methylglucose; AMP, adenosine monophosphate; ATP, adenosine triphosphate; CCB, cytochalasin B; CCD, cytochalasin D; CHAPS, 3-[(3-cholamidopropyl)dimethylammonio]-1-propanesulfonate; CHAPSO, 3-[(3-cholamidopropyl)dimethylammonio]-2-hydroxy-1-propanesulfonate; DDM, dodecyl maltoside; EDTA, ethylenediaminetetraacetic acid; HEPES, *N*-(2-hydroxyethyl)piperazine-*N*′-2-ethanesulfonic acid; FSK, forskolin, OG, octyl glucoside; RBC, red blood cell; SDS−PAGE, sodium dodecyl sulfate−polyacrylamide gel electrophoresis; Tris-HCl, tris(hydroxymethyl)aminomethane hydrochloride.

10.1021/bi015586w CCC: $20.00
Published on Web 11/29/2001

(see Discussion for details). More recently, we have shown that the human red cell sugar transporter presents sugar uptake and sugar exit sites simultaneously (*11*) and that the transporter presents at least two sugar uptake sites (*16*). These results are consistent with the simultaneous tetramer hypothesis which requires that the transporter presents two sugar uptake and two sugar exit sites at all times.

The present study asks whether the transporter exposes multiple sugar export sites. We show, by analysis of cytochalasin B binding to the e1 form of GluT1 and by analysis of cytochalasin B modulation of GluT1-mediated sugar transport, that the human red cell sugar transporter presents at least two e1 conformers simultaneously.

MATERIALS AND METHODS

Materials. Human blood was obtained from the American Red Cross. Radiochemicals were purchased from New England Nuclear (Boston, MA). All other reagents were purchased from Sigma Chemicals (St. Louis, MO).

Solutions. Saline consisted of 150 mM NaCl, 10 mM Tris-HCl, and 0.5 mM EDTA, pH 7.4. KCl medium consisted of 150 mM KCl, 10 mM HEPES, and 0.5 mM EDTA, pH 7.4. PBS consisted of 137 mM NaCl, 2.7 mM KCl, 8.1 mM Na_2HPO_4, and 1.7 mM $NaHPO_4$, pH 7.4. Lysis medium contained 10 mM Tris-HCl and 0.2 mM EDTA, pH 7.2. Stop solution consisted of ice-cold saline plus 10 μM CCB and 100 μM phloretin. Tris medium contained 50 mM Tris-HCl and 0.2 mM EDTA, pH 7.4.

Red Cells. Red cells were isolated from whole human blood by repeated wash/centrifugation cycles in ice-cold saline. One volume of whole blood was mixed with 3 volumes of saline and centrifuged at 10000*g* for 5 min at 4 °C. Serum and the buffy coat were aspirated, and the wash/centrifugation cycle was repeated until the supernatant was clear and a buffy coat was no longer visible.

Erythrocyte Membrane Ghosts. Washed red cells were lysed in 40 volumes of lysis medium, incubated on ice for 10 min, and then centrifuged at 22000*g* for 20 min at 4 °C. The supernatant was aspirated, and the lysis/centrifugation/aspiration cycle was repeated. The resulting membranes were resealed by incubation in KCl medium containing or lacking 4 mM Mg·ATP (pH 7.4) at 37 °C for 60 min and harvested by centrifugation at 22000*g* for 20 min at 4 °C.

Erythrocyte Membranes Depleted of Peripheral Membrane Proteins. Unsealed erythrocyte ghosts were exposed to 2 mM EDTA and 15.4 mM NaOH, pH 12 (0.8 mg of protein/mL of medium) for 10 min at 4 °C. Membranes were collected by centrifugation at 27000*g* for 20 min, and the pH of the membrane suspension was restored by three wash/centrifugation cycles each in 5 volumes of Tris medium. This procedure depletes red cell membranes of peripheral proteins (*17, 18*). The protein content of the membrane suspension was adjusted to 2 mg/mL using Tris medium, and the membranes were stored at −70 °C.

Purified Glucose Transport Protein. GluT1 containing endogenous lipid was purified from human erythrocyte membranes depleted of peripheral proteins by ion-exchange chromatography in octyl glucoside as described previously (*19*). Protein purity was verified by SDS−PAGE (*20*), and protein function was assessed by analysis of CCB binding capacity relative to protein content.

Equilibrium Cytochalasin B Binding. Red cells were depleted of endogenous sugars by incubation at 37 °C in 40 volumes of sugar-free saline. Cells were then resuspended in saline (4 °C) containing [^{3}H]CCB (6 μCi/mL), 10 μM CCD, and varying concentrations (5 nM to 50 μM) of unlabeled CCB. This suspension was incubated for 20 min at 4 °C, and [^{3}H]cytochalasin B binding was determined by a centrifugation procedure (*21*).

Briefly, pelleted, preincubated cells were resuspended by addition of 120 μL of medium containing [^{3}H]cytochalasin B. Aliquots (20 μL) of the suspension were counted by liquid scintillation spectroscopy using a Beckman scintillation counter. This provides a measure of "total" suspension [cytochalasin B]. Cells were incubated for 30 min at 4 °C with end-over-end rotation by which time equilibrium cytochalasin B binding is achieved (*10*). The cell suspension was centrifuged at 14000*g* for 20 s, and aliquots (20 μL) of the clear supernatant were counted by liquid scintillation spectroscopy. This provides a measure of "free" [cytochalasin B]. Bound [cytochalasin B] is computed as total − free [cytochalasin B]. All counts were quench corrected and expressed as disintegrations per minute. The same procedure was adopted for measuring cytochalasin B binding to peripheral protein-depleted red cell membranes and to purified human GluT1 proteoliposomes. Here, centrifugations were for longer time intervals (15 min) to ensure sedimentation of membranes and GluT1 proteoliposomes.

GluT1 Photolabeling Using [^{3}H]Cytochalasin B. Red cell membranes depleted of peripheral membrane proteins were resuspended in saline containing cytochalasin D (10 μM), [^{3}H]CCB (2.5 μM, 17 Ci/mmol), and ATP, AMP, or GTP (2 mM). The final protein concentration was 1 mg of total protein/mL. Suspensions were incubated for 10 min on ice and then irradiated on ice for 4 min at 280 nm using a Rayonet photochemical reactor (RPR-100). The membrane suspension was collected by centrifugation (14000*g* for 10 min), and the membrane pellet was subjected to two wash/centrifugation cycles in 40 volumes of PBS to remove free [^{3}H]CCB. The final pellet was resuspended in 1 mL of saline and assayed for protein content by the Pierce BCA procedure, and 50 μg of protein from each experimental condition was subjected to SDS−PAGE on a 10% gel (see below). Following electrophoresis, the gel was stained using Pro Blue and archived by quantitative digital scanning densitometry. Each lane was cut into 1.5 mm slices, and each slice was dissolved by overnight incubation in 30% hydrogen peroxide at 30 °C and counted for [^{3}H]CCB content by liquid scintillation spectroscopy (Beckman LS 6500 in auto DPM mode).

Glucose Carrier Labeling with 8-Azido[γ-^{32}P]ATP. Labeling was as described previously in (*22*). Briefly, 8-azido[γ-^{32}P]ATP in methanol was dried under N_2 and resuspended in 500 μL of Tris medium, pH 8.5 (90 μCi of ^{32}P, 10 μM final [azidoATP]). Purified GLUT1 proteoliposomes (500 μg of protein) were sedimented by centrifugation at 14000*g* for 20 min and combined with the methanol-free 8-azido-[γ-^{32}P]ATP solution. The suspension was incubated on ice for 30 min to ensure equilibrium ATP binding to GLUT1. Samples were placed in a plastic weigh boat on ice and irradiated for 90 s at 280 nm in a Rayonet photochemical reactor. Following UV irradiation (photolabeling), GLUT1 was washed three times to remove unbound 8-azido[γ-^{32}P]-

ATP by centrifugation (14000*g* for 15 min) and resuspended in 500 μL of Tris medium, pH 8.5. The effects of CCB on azidoATP binding to GLUT1 were examined by varying the [CCB] of the Tris medium over the range 0−2 μM during photolabeling. $MgCl_2$ was present at 5 mM in all experiments reported in this study.

Net 3-O-Methylglucose Uptake. Sugar transport by red cells was as described previously (*22*). Briefly, sugar-free cells or resealed erythrocyte ghosts at ice temperature were exposed to 5 volumes of ice-cold KCl medium containing [^{3}H]-3-*O*-methylglucose and variable concentrations of unlabeled 3-*O*-methylglucose and/or competing sugar. Uptake was measured over intervals of 15 s to 1 min; then 50 volumes (relative to cell volume) of ice-cold stopper solution was added to the cell/ghost suspension. Cells/ghosts were sedimented by centrifugation (14000*g* for 30 s), washed once in stopper, collected by centrifugation, and extracted in 500 μL of 3% perchloric acid. The acid extract was centrifuged, and duplicate samples of the clear supernatant were counted. Zero-time uptake points were prepared by addition of stopper to cells/ghosts prior to addition of medium containing sugar and radiolabel. Cells/ghosts were immediately processed. Radioactivity associated with cells/ghosts at zero time was subtracted from the activity associated with cells/ghosts following the uptake period. All uptakes were normalized to equilibrium uptake where cells/ghosts were exposed to sugar medium at 37 °C for 60 min prior to addition of stopper. Uptake assays were performed using solutions and tubes preequilibrated to 4 °C.

Dynamic Light Scattering. The hydrodynamic radii of detergent micelles, detergent/lipid micelles, and detergent/lipid/GluT1 micelles were determined at 24 °C by dynamic, laser light scattering and by Rayleigh light scattering by using a Precision Detectors PD2000 DLS in conjunction with a calibrated YMC Diol 300 column developed at 0.4 mL/min. All detergent solutions were prefiltered using 0.2 μm Sterile Acrodiscs. All samples (detergent micelles, detergent/lipid micelles, and detergent/lipid/GluT1 micelles) were cleared of large particulates by centrifugation at 4 °C at 170000*g* using a Beckman Airfuge followed by filtration through 0.2 μm Acrodiscs.

Analytical Procedures. Protein assays were carried out using the Pierce BCA protein assay procedure. SDS−PAGE was according to Laemmli (*20*). Kinetic solutions for equilibrium CCB binding to and 3MG transport by hypothetical carrier systems were obtained by making the rapid equilibrium assumption (*23*).

Curve Fitting Procedures and Kinetic Modeling. Kinetic parameters for equilibrium CCB binding and the concentration dependence of CCB inhibition of initial rates of 3MG transport were obtained by nonlinear regression using the software package KaleidaGraph 3.51 (Synergy Software, Reading, PA) and equations for ligand binding and sugar transport as presented in the Appendix.

RESULTS

Cytochalasin B Binding. The concentration dependence of equilibrium cytochalasin B binding to human red blood cells is shown in Figure 1A. Although the relationship between equilibrium $[CCB]_b$ and $[CCB]_f$ appears to follow simple saturation kinetics, close inspection (see the Scatchard plot inset of Figure 1A) reveals systematic deviations from simple behavior at both low and high $[CCB]_f$. This behavior is more pronounced with measurements of equilibrium CCB binding to purified GluT1 proteoliposomes (Figure 1B). CCB binding to GluT1 increases monotonically with [CCB] at high ligand concentrations but cooperatively with [CCB] at very low [CCB] (see inset to Figure 1B). The linear dependence of binding on [CCB] at high ligand concentrations appears to result from nonspecific ligand binding because phloretin [100 μM, a potent inhibitor of CCB binding (*10*, *24*)] does not inhibit this component of binding (Figure 1B). However, binding at low [CCB] is inhibited by phloretin.

CCB binding to RBC integral membrane proteins (Figure 1C,D,E) also deviates from simple saturation kinetics. At low $[CCB]_f$, binding appears to show positive cooperativity (see Scatchard plot insets of Figure 1C,D). The presence of Mg·ATP (4 mM) appears to inhibit cooperativity and to increase CCB binding at low ligand concentrations (Figure 1D,E). This may explain why CCB binding to intact red cells which contain approximately 2 mM ATP (*22*) shows less cooperativity than binding to ATP-free, purified GluT1.

To examine this further, we photolabeled RBC integral membrane proteins using [^{3}H]CCB by UV cross-linking in the presence and absence of ATP and the CCB binding inhibitor phloretin (100 μM). Photolabeled membranes were washed to remove free radioligand, and proteins were resolved by SDS−PAGE. Individual gel lanes were stained, subjected to densitometric analysis of protein content, and then sliced into 1.5 mm segments, dissolved, and counted for associated radioligand. Figure 2 shows that the major labeled proteins are resolved as proteins of M_r 55000−70000. This corresponds to the mobility of human GluT1 (*22*). Phloretin (100 μM) blocks [^{3}H]CCB photoincorporation into these proteins by 70−100-fold. Our initial measurements demonstrated that ATP (2 mM) increased [^{3}H]CCB photoincorporation into RBC GluT1 by only 10%. Because the wavelength for maximum photoincorporation of [^{3}H]CCB into GluT1 [280 nm (*25*)] overlaps significantly with the absorbance spectrum of ATP, it is possible that absorbance of the exciting light by ATP (an inner filter effect) reduces the efficiency of GluT1 photolabeling. Inhibition of [^{3}H]CCB photoincorporation into GluT1 was observed using 2 mM GTP (data not shown), a nucleotide known not to interact with the glucose transport protein (*26*). However, GTP and ATP absorbance spectra are not sufficiently close to permit the use of GTP as an inner-filter control for ATP modulation of CCB photolabeling of GluT1. In contrast, the absorbance spectra of 2 mM AMP and ATP over the range $\lambda = 260-310$ nm are indistinguishable. AMP, in contrast to ATP, reduces phloretin-inhibitable [^{3}H]CCB photoincorporation into RBC membrane proteins by 50% (Figure 2). Earlier studies have shown that AMP does not modulate GluT1 structure or function but does serve as a competitive inhibitor of ATP binding to GluT1 (*27*). These findings suggest that ATP enhances (relative to the action of AMP) [^{3}H]CCB binding to GluT1. This result was confirmed in equilibrium CCB binding measurements using RBC integral membrane proteins. AMP is without effect on equilibrium CCB binding to membranes (Figure 1E).

ATP Binding. If ATP modulates CCB binding to GluT1, does CCB modulate ATP interaction with the glucose transporter? To examine this question, we photolabeled

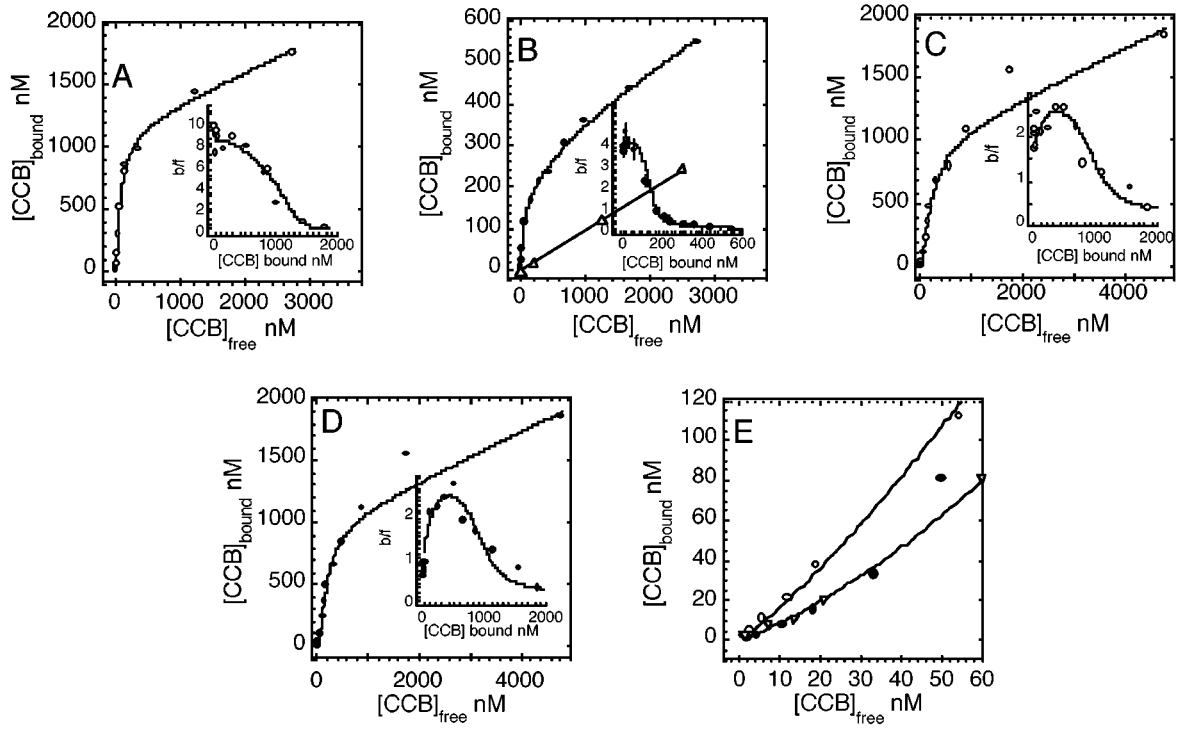

FIGURE 1: Cytochalasin B binding to human GluT1. (A) Cytochalasin B binding to human RBCs. Ordinate: concentration of bound CCB in nanomolar. Abscissa: free [CCB] in nanomolar. Each data point represents the average of measurements made in duplicate in at least three separate experiments. The curve drawn through the points was calculated by nonlinear regression according to eqs 5−7 in which the following parameters were obtained: [GluT1] = 1156 nM, K_L = 147 nM, α = 0.39, and χ = 0.24. The inset shows the same data set plotted in Scatchard form as $[CCB]_{bound}/[CCB]_{free}$ versus $[CCB]_{bound}$. (B) Cytochalasin B binding to GluT1 proteoliposomes. Ordinate: concentration of bound CCB in nanomolar. Abscissa: free [CCB] in nanomolar. Binding is shown in the absence (●) and presence (△) of 100 mM phloretin. Each data point represents the average (±SEM) of measurements made in duplicate in at least three separate experiments. The curve drawn through the control points (●) was calculated by nonlinear regression according to eqs 5−7 in which the following parameters were obtained: [GluT1] = 161 nM, K_L = 253 nM, α = 1.56, and χ = 0.098. The inset shows the same data set plotted in Scatchard form as $[CCB]_{bound}/[CCB]_{free}$ versus $[CCB]_{bound}$. The line drawn through the phloretin-inhibited points (△) was computed by linear regression according to eq 5 where χ = 0.098. (C) Cytochalasin B binding to human RBC integral membrane proteins in the presence of 2 mM Mg·ATP. Ordinate: concentration of bound CCB in nanomolar. Abscissa: free [CCB] in nanomolar. Each data point represents the average of measurements made in duplicate in at least three separate experiments. The curve drawn through the points was calculated by nonlinear regression according to eq 8 in which the following parameters were obtained: [GluT1] = 950 nM, K_L = 700 nM, K_N = 50 μM, α = 0.1, $\epsilon = \varphi = \sigma$ = 5, ω = 0.7, and χ = 0.2. The inset shows the same data set plotted in Scatchard form as $[CCB]_{bound}/[CCB]_{free}$ versus $[CCB]_{bound}$. (D) Cytochalasin B binding to human RBC integral membrane proteins in the absence of ATP. Ordinate: concentration of bound CCB in nanomolar. Abscissa: free [CCB] in nanomolar. Each data point represents the average of measurements made in duplicate in at least three separate experiments. The curve drawn through the points was calculated by nonlinear regression according to eq 8 in which the following parameters were obtained: [GluT1] = 841 nM, K_L = 1118 nM, α = 0.034, and χ = 0.2. The inset shows the same data set plotted in Scatchard form as $[CCB]_{bound}/[CCB]_{free}$ versus $[CCB]_{bound}$. (E) Cytochalasin B binding to human RBC integral membrane proteins in the absence of ATP (●), in the presence of 2 mM ATP (○), and in the presence of 2 mM AMP (▽). Ordinate: concentration of bound CCB in nanomolar. Abscissa: free [CCB] in nanomolar. Experiments were carried out as paired experiments with 0 M ATP as the control condition, and each point represents the average of measurements made in duplicate in at least three separate experiments. The curves drawn through the points were calculated by nonlinear regression according to eq 8 in which the following parameters were obtained. 2 mM ATP: [GluT1] = 950 nM, K_L = 744 nM, K_N = 57 μM, α = 0.1, $\epsilon = \varphi = \sigma$ = 5, ω = 0.7, and χ = 0.2. 0 M ATP and 2 mM AMP: [GluT1] = 941 nM, K_L = 1580 nM, α = 0.034, and χ = 0.2.

purified GluT1 proteoliposomes with [γ-^{32}P]azidoATP in the presence and absence of CCB or its inactive analogue cytochalasin D (CCD). We have previously shown that GluT1 lacks ATPase activity and that azidoATP is a useful probe of the GluT1 nucleotide binding domain (*22*, *27*). Figure 3 shows that CCB but not CCD increases azidoATP photoincorporation into isolated human GluT1 protein.

Effect of ATP on GluT1 Quaternary Structure. We have previously demonstrated that both CCB and ATP binding to GluT1 are sensitive to GluT1 quaternary structure (*19*, *22*, *28*, *29*). We were interested, therefore, in determining whether ATP binding to GluT1 also modulates GluT1 quaternary structure. Purified GluT1 was solubilized in several detergents in the presence and absence of 2 mM Mg·ATP. The solubilized protein was clarified by centrifugation at 170000*g* for 30 min at 4 °C and then filtered through 0.2 μm membrane filters to remove any remaining particulate material. The resulting micelles were subjected to hydrodynamic size analysis at 24 °C by dynamic light scattering, by Rayleigh light scattering, or by size-exclusion chromatography. Figure 4 shows that GluT1 solubilized in 40 mM octyl glucoside forms micelles of average Stokes or hydrodynamic radius (Rh) of 8.5 nm that are stable over a period of 2 days at 24 °C. As with cholic acid-solubilized GluT1 (*28*), addition of 2 mM dithiothreitol causes a rapid decrease in particle size ($t_{1/2}$ = 60 min) to 6.7 nm. Mg·ATP (2 mM) is without effect on GluT1/lipid/detergent micelle size. Octyl glucoside micelles are characterized by an Rh of 1.75 nm. Assuming

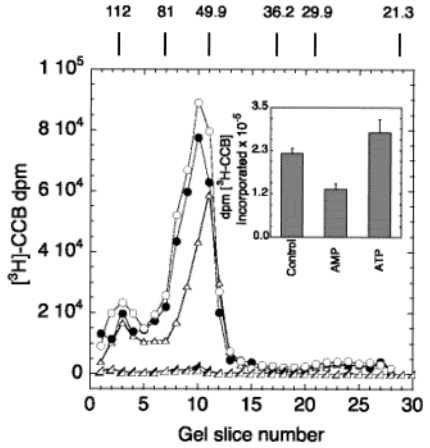

FIGURE 2: Effect of AMP and ATP on GluT1 photolabeling by [^{3}H]CCB. Ordinate: dpm of [^{3}H]CCB incorporated into membrane proteins. Abscissa: SDS−PAGE slice. Integral membrane proteins were photolabeled with [^{3}H]CCB in the absence (●, ○, △) or in the presence of the sugar uptake site ligand phloretin (100 μM, tilted ▲ and tilted △). Cells were also exposed to 2 mM ATP (○, tilted △), to 2 mM AMP (△), or to 0 M nucleotide (●, tilted ▲) prior to and during photolabeling. After irradiation, membranes were harvested, washed in label-free medium, and resolved by SDS−PAGE. Each lane was cut into 2 mm slices which were counted. The mobility of molecular mass standards (kDa) is indicated by the markers above the data points. The inset summarizes the results of three separate experiments quantitating dpm of [^{3}H]CCB incorporated into GluT1 in the absence (control) or presence of AMP or ATP. Results are shown as the mean ± SEM. The results with AMP are significantly less than with the control (one-tailed *t*-test, $p < 0.04$) while the results with ATP are signifcantly greater than with the control (one-tailed *t*-test, $p < 0.05$) and AMP (one-tailed *t*-test, $p < 0.01$).

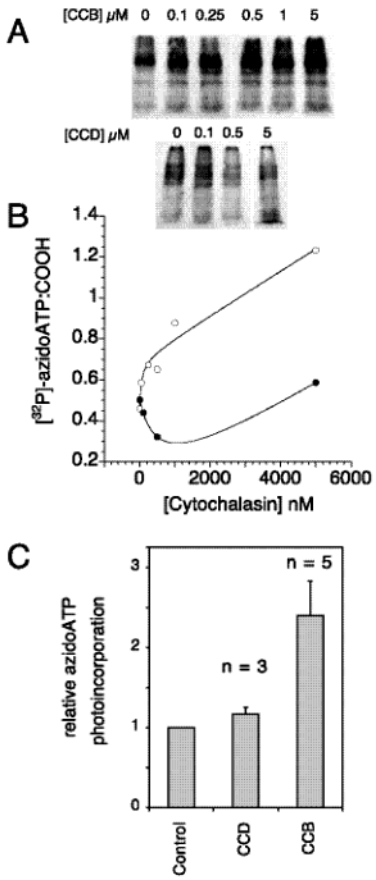

FIGURE 3: Effects of cytochalasins on GluT1 photolabeling by [γ-^{32}P]azidoATP. (A) Purified GluT1 (100 μg) was exposed in the dark (on ice) to 10 μM [γ-^{32}P]azidoATP in the presence of increasing concentrations of CCB (○) or CCD (●) for 30 min. Membranes were then irradiated at 300 nm for 2 min, harvested, washed in isotope-free saline, resolved by SDS−PAGE, and transferred to Immobilon membranes where they were probed for GluT1 content by immunoblot analysis using a luminescence/anti-GluT1 carboxterminal peptide antibody assay and for [γ-^{32}P]-azidoATP by autoradiography. The digitized [γ-^{32}P]azidoATP autoradiograms are shown above the line graph. (B) Quantitation of the data in panel A. Ordinate: relative photoincorporation of [γ-^{32}P]azidoATP into human red blood cell GluT1. Abscissa: [cytochalasin] in nanomolar. [γ-^{32}P]azidoATP content (detected by autoradiography) that comigrated with GluT1 (as detected by immunoblot analysis) and GluT1 content were quantitated by scanning digital densitometry and expressed as the ratio [γ-^{32}P]-azidoATP:[GluT1]. This ratio is plotted in the figure versus [cytochalasin]. The curves drawn through the points have no theoretical significance. (C) Summary of experiments in which the effect of 5 μM CCB (five experiments) or CCD (three experiments) on GluT1 photoincorporation of azidoATP was measured. Ordinate: azidoATP photoincorporation relative to the control. Results are shown as the mean ± SEM. The results with CCD are not significantly different from those of the control (one-tailed *t*-test, $p > 0.09$) while the results with CCB are signifcantly greater than those of the control (one-tailed *t*-test $p < 0.015$) and CCD (one-tailed *t*-test, $p < 0.03$).

an octyl glucoside van der Waals volume of 350 cm^3/mol, this micellular Stokes radius is consistent with a detergent aggregation number of 40 molecules.

Cholic acid forms stable GluT1/detergent micelles of Rh = 8 nm. Dodecyl maltoside solubilization of GluT1 initially produces protein/lipid/detergent micelles of Rh = 9.8 nm, but upon warming to 24 °C, these particles decay to Rh = 5.3 nm with a half-time of 2 h. Addition of 2 mM DTT rapidly accelerates this decay process ($t_{1/2}$ = 7 min), but Mg·ATP is without effect on particle dissociation. Dodecyl maltoside and dodecyl maltoside/lipid micelles are characterized by an Rh of 2.4 and 3.6 nm, respectively. Table 1 shows that other detergents (CHAPS, CHAPSO, Triton X-100, and digitonin) produce only small GluT1/detergent micelles. When CHAPS/GluT1/lipid micelles (Rh = 4.5 nm) are dialyzed against detergent-free buffer and the resulting proteoliposomes are then resolubilized in 40 mM octyl glucoside, the resulting micelles are characterized by an Rh of 9 nm.

These findings suggest that some detergents stabilize higher GluT1 aggregation states while others promote formation of GluT1 oligomers of smaller aggregation states, a process enhanced by inclusion of reductant. ATP appears to be without effect on GluT1 aggregation state in detergent.

CCB Modulation of Sugar Transport by Red Blood Cells. Our previous studies have shown that the human red blood cell glucose transporter presents at least two, interacting extracellular maltose binding sites and that occupation of the high-affinity site by maltose increases uptake of the transported sugar 3-*O*-methylglucose (3MG) through the remaining import site (*16*). We were curious, therefore, to determine whether the multiple, interacting GluT1 CCB binding sites detected by equilibrium CCB binding would have a similar action on 3MG uptake by red cells. Figure 5A demonstrates that uptake of 100 μM 3MG by human red blood cells at 4 °C is stimulated by low (<20 nM) [CCB] but is inhibited by higher concentrations of CCB. CCD is

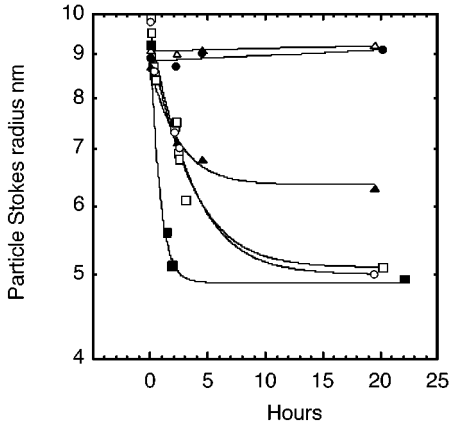

FIGURE 4: Effects of detergents, reductant, and ATP on the hydrodynamic (Stokes) radius of GluT1/lipid/detergent micelles as measured by dynamic light scattering. Ordinate: micelle hydrodynamic radius (nm; note the logarithmic scale). Abscissa: time in hours. GluT1 proteliposomes were solubilized in 40 mM octyl glucoside (△, ▲, ●) or in 40 mM dodecyl maltoside (□, ■, ○) at ice temperature. At zero time, micelles were warmed to 24 °C in the presence (▲, ■) or absence (△, □) of 2 mM DTT or 2 mM ATP (●, ○). The curves drawn through the data points were computed by nonlinear regression assuming simple exponential decay of particle size from a starting point to a final value; i.e., the Stokes radius is given by $S_r = M + \rho e^{-kt}$, where M is the final Stokes radius, ρ is the change in the Stokes radius, k is the first-order rate constant describing the rate of decay, and t is time. The following results were obtained: OG (0 M DTT, 0 M ATP), M = 9.05 nm and ρ = 0 nm; OG (2 mM DTT, 0 M ATP), M = 6.35 nm, ρ = 2.33 nm, and k = 0.44/h; OG (0 M DTT, 2 mM ATP), M = 8.84 nm and ρ = 0 nm; DDM (0 M DTT, 0 M ATP), M = 5.1 nm, ρ = 4.1 nm, and k = 0.33/h; DDM (2 mM DTT, 0 M ATP), M = 4.9 nm, ρ = 4.3 nm, and k = 1.39/h; DDM (0 M DTT, 2 mM ATP), M = 5.0 nm, ρ = 4.47 nm, and k = 0.33/h. Data points represent the average of at least three separate determinations.

Table 1: Properties of Various Detergents and GluT1/Detergent Micelles[a]

detergent species	particle hydrodynamic radius, Rh (nm)			
	detergent alone	detergent + lipid	detergent + lipid + GluT1	detergent + lipid + GluT1 + DTT
cholic acid	1 ± 0	na[b]	8.0 ± 0.6 (7.8)[c]	5.7 ± 0.1 (6.1)
CHAPS	1.6 ± 0.1	na	4.5 ± 0.8	na
CHAPSO	1.2 ± 0.1	na	3.9 ± 0.2	na
n-octyl β-D-gluco-pyranoside	1.8 ± 0.1	na	8.5 ± 0.1 (8.9)	6.7 ± 0.1 (6.5)
n-dodecyl β-D-malto-side	2.4 ± 0.1	3.6 ± 0.2	9.2 ± 0.3[d] 5.6 ± 0.3	5.3 ± 0.2
digitonin	3.9 ± 0.2	na	4.5 ± 0.2	na
Triton X-100	3.7 ± 0.1	na	6.1 ± 0.1	na

[a] The Stokes radii (Rh, nm) of micelles formed from ionic, zwitterionic, and nonionic detergents were analyzed by dynamic laser light scattering. Results shown in parentheses were obtained by size-exclusion chromatography over a calibrated YMC Diol 300 column. Concentrations of detergents were 40 mM (cholic acid, octyl glucoside, dodecyl maltoside), 20 mM (CHAPS, CHAPSO), or 0.5% (w/v, Triton X-100, digitonin). GluT1 (200 μg of protein + 200 μg of red cell lipids ± 2 mM DTT) was solubilized in 800 μL of phosphate-buffered saline (4 °C) containing detergent. All samples were precleared by centrifugation at 140000*g* for 30 min at 4 °C and were filtered through a 0.2 μm filter prior to DLS analysis at 24 °C. [b] These measurements were not made. [c] Values in parentheses were obtained by size-exclusion chromatography. [d] All measurements were made at 24 °C with the exception of this determination which was made at 4 °C. Results are shown as the mean ± SEM of at least three determinations.

without effect on 3MG uptake. A second e1-conformation-specific GluT1 ligand, forskolin (FSK), also stimulates 3MG uptake by red cells at low FSK concentrations but inhibits uptake at higher [FSK] (Figure 5A). Similar studies with resealed red cell ghosts show that removal of intracellular ATP shifts the [CCB] dose response of transport stimulation to higher [CCB] (Figure 5B).

If stimulation of 3MG uptake by cis (e.g., extracellular maltose) or trans (intracellular CCB) ligands requires functional cooperativity between glucose transporter subunits, stimulation should be lost when the GluT1 tetramer is forced to dissociate by exposure to dithiothreitol (*30*, *31*). Figure 6 shows that exposure of human red blood cells to 2 mM DTT reduces net 3MG uptake as reported previously (*30*) but also inhibits stimulations of 3MG uptake by low concentrations of extracellular maltose or by CCB.

DISCUSSION

The present study asks whether the human erythrocyte glucose transporter presents multiple sugar exit sites and, if so, are these sites modulated by ATP? We examine whether sugar exit and nucleotide binding site interactions are affected by GluT1 quaternary structure, and we ask whether GluT1 oligomeric structure is affected by ATP. Our findings are consistent with the hypothesis that the human red blood cell sugar transporter is a GluT1 oligomer which presents multiple interacting sugar exit and nucleotide binding sites. Sugar transporter oligomeric structure seems not to be affected by removal of intracellular ATP.

Our analysis of sugar transport exit site availability is based on the use of the exit site ligands cytochalasin B and forskolin. By examining cytochalasin B binding to the glucose transporter or cytochalasin B inhibition of sugar transport, it is possible to determine whether one or more cytochalasin B binding sites exist in any given transporter at any instant. However, this analysis assumes that cytochalasin B and forskolin bind to the glucose transporter exit site.

This assumption is supported by several lines of evidence. Intracellular glucose is a competitive inhibitor of cytochalasin B and forskolin binding to GluT1 (*10*, *32*). Cytochalasin B and FSK act as competitive inhibitors of glucose exit but act as noncompetitive inhibitors of glucose entry (*33*, *34*). CCB and FSK binding are also mutually exclusive (*35*). These observations confirm that the CCB/FSK site and the sugar exit site are mutually exclusive. However, they do not prove that these sites are identical because a competitive inhibitor can inhibit substrate binding by (1) competing for the same site, (2) steric hindrance, (3) sharing a common binding group on the enzyme, (4) having distinct but overlapping sites, or (5) binding at a distinct site that promotes conformational changes in the substrate site and vice versa (*36*). In the absence of a GluT1−ligand pair structure, this question must remain unanswered. Nevertheless, the correlation between CCB binding site and exit site accessibility validates the use of CCB binding as a quantitative measure of exit site availability.

The evidence supporting multiple exit (CCB binding) sites is 2-fold. (1) CCB binding to isolated GluT1 and to red cell

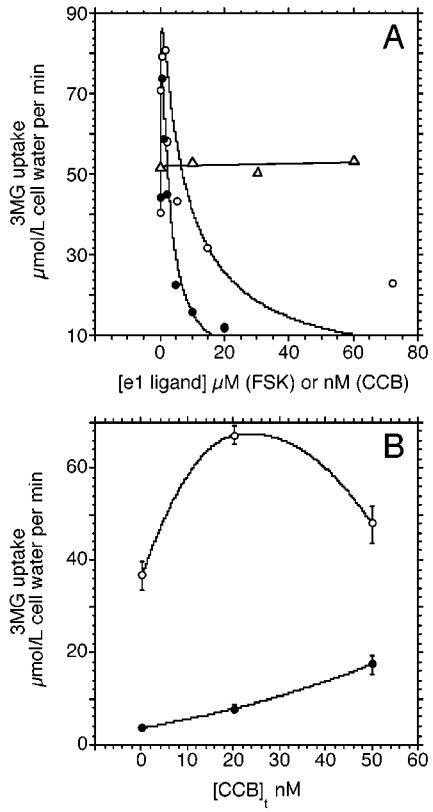

FIGURE 5: (A) Effects of cytochalasin B (○), CCD (△), or forskolin (●) on the initial rate of 100 μM 3MG uptake by human red blood cells at 4 °C. Ordinate: initial rate of 3MG uptake in μmol (L of cell water)$^{-1}$ min^{-1}. Abscissa: [CCB] (in nanomolar) or [FSK] (in micromolar). Each CCB data point represents the average of at least six separate experiments made in triplicate. Each FSK data point represents the average of at least three separate experiments made in triplicate. The curves drawn through the points were computed by nonlinear regression analysis using eq 4 and the relationship, rate of sugar uptake, $v = \tau S$. The following results were obtained: CCB, $K = 110$ μM, $K_L = 40$ nM, $v_1 = 12$ μmol L^{-1} min^{-1}, $v_2 = 15$ μmol L^{-1} min^{-1}, $v_3 = 110$ μmol L^{-1} min^{-1}, $v_4 = 135$ μmol L^{-1} min^{-1}, $\alpha = 0.03$, $\beta = 0.7$, $\gamma = 0.3$; FSK, $K = 110$ μM, $K_L = 2$ μM, $v_1 = 9$ μmol L^{-1} min^{-1}, $v_2 = 10$ μmol L^{-1} min^{-1}, $v_3 = 40$ μmol L^{-1} min^{-1}, $v_4 = 70$ μmol L^{-1} min^{-1}, $\alpha = 0.25$, $\beta = 0.6$, $\gamma = 0.6$. (B) Effects of ATP removal on CCB modulation of 3MG uptake. 3MG uptake was measured in intact cells (○) and in ATP-free red cell ghosts (●). Ordinate: rate of 3MG uptake at ice temperature [μmol (L of cell water)$^{-1}$ min^{-1}]. Abscissa: $[CCB]_{total}$ in nanomolar. Each point represents the mean ± SEM of three separate measurements.

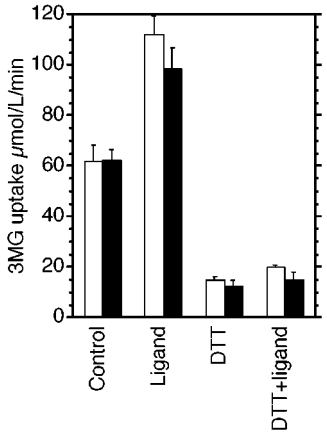

FIGURE 6: Effect of reductant on 3MG uptake and its stimulation by maltose (open bars) or by CCB (filled bars). Ordinate: 3MG uptake in μmol (L of cell water)$^{-1}$ min^{-1}. Abscissa: control cells, cells exposed to ligand (0.5 mM maltose or 20 nM CCB), control cells exposed to 2 mM DTT, and cells exposed to 2 mM DTT and ligand (0.5 mM maltose or 20 nM CCB). Results are shown as the SEM of three separate determinations in quadruplicate.

membranes is consistent with at least two populations of sites that interact with positive cooperativity. (2) As the CCB concentration applied to red cells is increased, CCB first stimulates and then inhibits 3MG uptake. We believe that these effects have not been reported previously due to the very low ligand concentrations required to elicit these results. CCB interaction with a non-GluT1 protein such as actin [a known CCB binding protein (*37*)] might also account for this result. Several arguments refute this hypothesis. CCB binding studies were carried out in the presence of saturating CCD, a competitive inhibitor of CCB binding to actin [but not to GluT1 (*38*)]. Thus the binding measurements do not include significant binding to actin. CCD does not mimic the ability of CCB to modulate transport. Solubilization of red cell membranes by nonionic detergents releases >99% of membrane resident GluT1 but leaves actin behind in the cytoskeletal shell (*39*), indicating that GluT1 and actin do not interact directly to modulate glucose transport. Forskolin mimics the ability of CCB to stimulate and then inhibit red cell 3MG uptake but does not interact with actin (*40*).

Our experiments investigating CCB binding to red cell membranes in the presence of ATP suggest that ATP reduces cooperativity between CCB binding sites, increases the intrinsic affinity of exit sites for CCB, but leaves the total number of CCB binding sites unchanged. The net effect is that ATP increases bound [CCB] at low [CCB]. The observation that ATP increases [^{3}H]CCB photoincorporation into human GluT1 relative to the effect of AMP [a nucleotide that does not modulate sugar transport (*27*)] is consistent with this hypothesis. While it is possible that ATP/GluT1 interaction simply increases the efficiency of GluT1 photolabeling by CCB, it is interesting to note that CCB also increases photoincorporation of [γ-^{32}P]azidoATP into GluT1. This suggests that CCB and ATP binding sites interact with positive cooperativity. This is especially interesting because intracellular ATP serves to increase $K_{m(app)}$ for glucose exit (*41*), indicating that ATP differentially modulates the binding of e1 ligands. This conclusion may be an oversimplification, however, because $K_{m(app)}$ for glucose transport is a complex product of both binding and translocation steps (*42*).

Given this cooperativity between nucleotide and CCB binding sites and our previous demonstrations that nucleotide (*22*) and CCB (*30*) binding to GluT1 are affected by reductant-promoted tetrameric GluT1 dissociation into dimers, we were interested in understanding whether ATP binding to GluT1 affected GluT1 quaternary structure. Our studies of GluT1/detergent/lipid micelle hydrodynamic radius by dynamic light scattering demonstrate that GluT1 quaternary structure is sensitive to the presence of reductant and to the nature of the solubilizing detergent but that the presence of ATP is without effect on GluT1/lipid/detergent micelle size or stability.

GluT1 forms particles of 8−10 nm hydrodynamic radius when solubilized in octyl glucoside or cholic acid. This particle size is consistent with the results of previous studies suggesting an aggregation state of 4 GluT1 (*19*, *28*). Dodecyl

maltoside promotes GluT1 dissociation into a smaller particle, a process accelerated by the presence of reductant. Zwitterionic detergents (CHAPS and CHAPSO) produce only small GluT1/detergent/lipid micelles. The effects of CHAPS and dodecyl maltoside on GluT1 quaternary structure are reversible because detergent removal by dialysis followed by resolubilization in octyl glucoside or cholic acid results in the generation of GluT1/detergent/lipid micelles of Rh = 9 nm. These particle sizes were also confirmed using size-exclusion chromatography and Rayleigh light scattering. The latter technique also permits direct computation of the GluT1/detergent/lipid micelle mass. In the presence of OG and absence of reductant, the mass of the GluT1/detergent/lipid micelle is 0.40 MDa. Addition of reductant reduces this mass to 0.17 MDa. Assuming 23 lipid molecules per GluT1 protein (*43*), these masses are consistent with a composition of 4 GluT1 and 460 detergent molecules (or 5 GluT1 and 240 detergent molecules) per large micelle and 2 GluT1 and 130 detergent molecules per small micelle. A previous study (*44*) has concluded that GluT1 is monomeric in glycol *n*-dodecyl ether. The reasons for these different conclusions are unclear.

Although GluT1 quaternary structure is unaffected by ligand binding, the reverse is certainly not the case. Human red cell treatment by extracellular reductant causes GluT1 reduction and dissociation into GluT1 dimers (*30*). In the present study we also show that RBC treatment with reductant results in the loss of maltose stimulation of 3MG uptake by red cells. This is consistent with the hypothesis that subunit interactions are required for maltose or CCB stimulation of 3MG transport and that reductant-promoted tetrameric GluT1 dissociation into dimers results in the loss of functional cooperativity between subunits (*19*).

A Model for Glucose Transport. Each GluT1 protein is proposed to function as a ping-pong (iso-uni-uni) carrier (*1*) that alternates between two states, e1 presenting an exit site and e2 presenting an import site (*45*, *46*). Conformational changes between substrate-liganded forms of e2 and e1 states catalyze sugar translocation. We propose (see Figure 7) that the human red blood cell glucose transporter complex contains four GluT1 proteins (subunits) arranged as a pair (cis and trans) of interacting GluT1 dimers. Subunit interactions within each dimer prevent subunits from adopting identical conformational states. If one subunit in a dimer presents an exit site, the other (cis) subunit must present an import site and vice versa. In this way, each transporter complex exposes two import and two export sites at any instant.

Supporting Physical and Functional Evidence. Jung has demonstrated that the transporter in human red blood cells has a radiation target size consistent with that of a GluT1 dimer or a GluT1 tetramer (*47*). GluT1 isolated from human red blood cells in the absence of reductant and solubilized in cholic acid exists as a noncovalent, GluT1 homotetramer (*19*). Chemical cross-linking of nonreduced GluT1 and red cell-resident GluT1 indicates the presence of GluT1 dimers and tetramers (*19*, *28*). GluT1 purification in the presence of reductant or exposure of nonreduced purified GluT1 to reductant causes transporter dissociation into GluT1 dimers (*19*, *28*). Freeze-fracture EM shows that the reduced glucose transport protein forms a 6 nm diameter intramembranous particle that most likely represents a GluT1 dimer (*45*, *48*) while nonreduced transporter forms larger 10 nm particles consistent with a GluT1 tetramer (*48*). Transporter oligomeric structure sensitivity to the presence of reductant appears to result from the presence of a single, internal disulfide bridge within each GluT1 protein (*30*). Cysteine mutagenesis of GluT1 and N-terminal sequence analysis of peptides derived from differentially carboxymethylated, purified GluT1 indicate that GluT1 cysteines 347 and 421 of putative transmembrane domains 8 and 11 are the most probable candidate residues involved in internal disulfide bridge formation (*30*).

Reduced GluT1 solubilized by and purified in the presence of glycol *n*-dodecyl ether is resolved as a monomer by size-exclusion chromatgography (*44*) but as a tetramer when solubilized in cholic acid (*19*, *28*). The anion transporter (*49*), the oligosaccharyltransferase (*50*), and the heterotrimeric Sec61p complex of the protein-conducting channel of the endoplasmic reticulum membrane (*51*) are other examples of multiprotein or multisubunit membrane complexes that dissociate and/or lose activity when low molecular weight, nonionic detergents (e.g., octyl glucoside) are employed. Interestingly, octyl glucoside stabilizes higher order GluT1 aggregation states while dodecyl maltoside and glycol *n*-dodecyl ether do not (see here and ref *44*).

Kinetic analysis indicates that reduced GluT1 behaves as if comprised of two functionally independent ping-pong carriers (*19*, *52*, *53*). The anion exchanger (*54*) and the aquaporin water channel (*55*) of human red cells, the aquaglyceroporin channel (*56*), the NKCCl cotransporter (*57*), the TetA (tetracycline cation/proton) antiporter (*58*, *59*), the renal NHE1 (Na/H) antiporter (*60*), the NhaA Na^+/H^+ antiporter (*61*, *62*), and the LacS H^+/lactose symporter (*63*) are also comprised of multiple copies of functional subunits. Ligand binding studies demonstrate that the nonreduced form of the glucose transporter most closely resembles that found in intact cells (*9*−*11*) presenting e1 (cytochalasin B reactive) and e2 (extracellular sugar reactive) states simultaneously. Exposure to extracellular reductant depresses red cell sugar transport rates, converts the transporter's ligand binding properties to those expected of a ping-pong carrier, and causes transporter dissociation into GluT1 dimers (*19*, *28*, *30*).

Several studies report fully functional Cys-less GluT1 (relative to wild-type GluT1) in *Xenopus laevis* oocytes (*64*−*70*). However, unlike GluT1 expressed in human (*31*), rat, and avian red cells (*34*), human 3T3L1 adipocytes (*71*, *72*), Cos-7 cells (*73*), CHO cells (*30*), and HEK293 and K562 cells,[2] GluT1 expressed in *X. laevis* oocytes does not interact with antibodies directed against tetrameric GluT1 (*30*) and is not inhibited by extracellular reductant (*30*, *66*). This suggests that GluT1 expressed in *X. laevis* oocytes may be dimeric. Reduced, red cell-resident and reconstituted human GluT1 are functional (*30*, *74*, *75*), but comparison with nonreduced red cell-resident GluT1 (*76*) confirms that reduced GluT1 has a 10-fold lower catalytic turnover (see here and refs *77* and *78*).

Details of the Model. Our previous studies have demonstrated that low extracellular [maltose] increases both 3MG uptake by and CCB binding to human red cell GluT1 (*16*). We hypothesized that, in the absence of maltose, the affinity

[2] K. Levine, E. K. Cloherty, and A. Carruthers, unpublished observations.

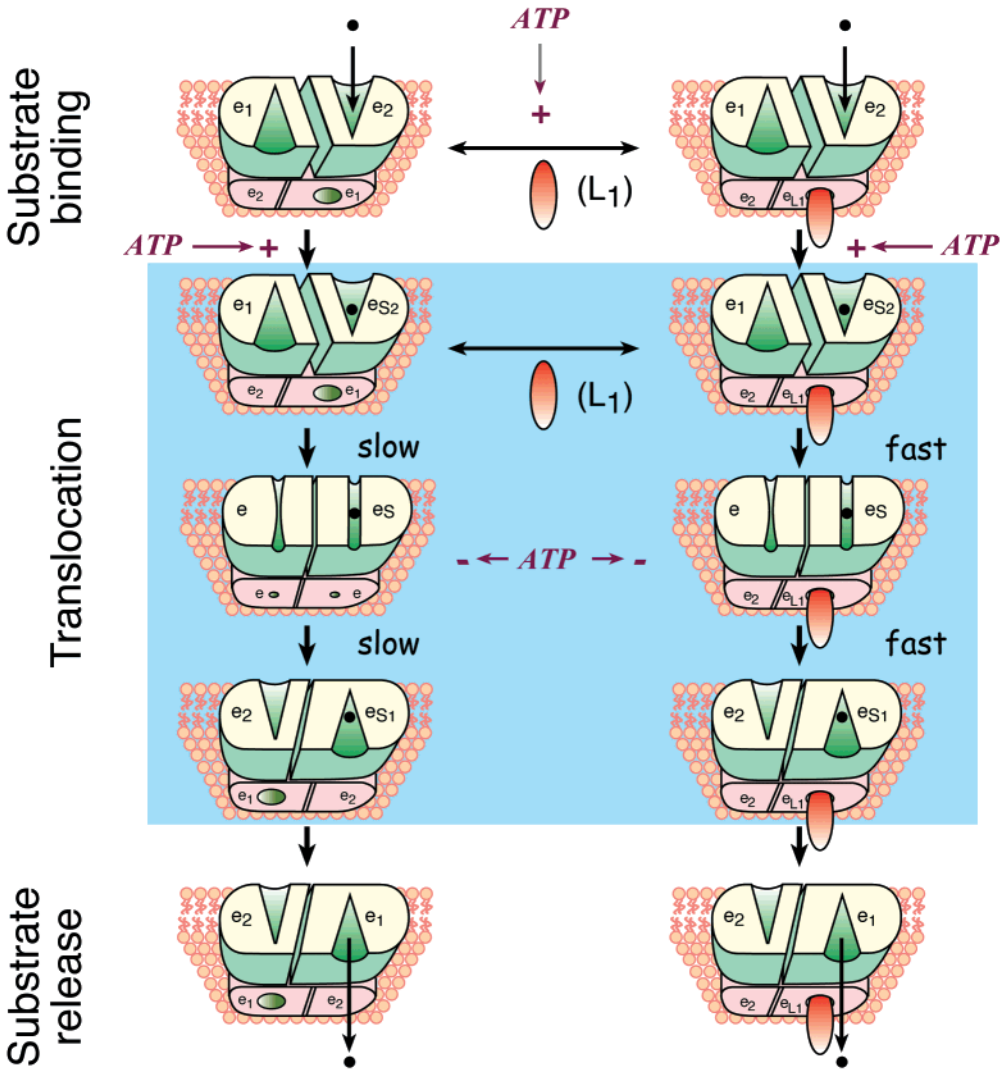

FIGURE 7: A model for CCB modulation of red blood cell sugar transport. The glucose transporter is shown schematically as a GluT1 tetramer in the membrane lipid bilayer. The region above the bilayer represents the cell's exterior and the region below the cytosol. The tetramer is a dimer of GluT1 dimers. The frontmost dimer is sectioned through the catalytic center to reveal that one subunit has adopted an e1 conformation presenting a sugar exit site and the other has adopted an e2 conformation presenting a sugar uptake site. This dimer is thus an (e1•e2) conformer. The rearmost dimer is an (e2•e1) conformer. In the absence of CCB (L_1), the frontmost dimer would normally bind extracellular sugar (S2) to form an (e1•eS2) conformer, and the entire complex can slowly undergo the (e1•eS2)(e2•e1) to (e2•eS1)-(e1•e2) conformational change, resulting in release of sugar at the cytosolic surface of the membrane. When CCB binds to the (e1•e2)-(e2•e1) complex, S2 binding to the trans dimer may now proceed with higher affinity, or prebinding S2 to (e1•e2)(e2•e1) to form the (e1•eS2)(e2•e1) conformer promotes high-affinity CCB binding to the rearmost dimer. In both instances, sugar translocation [the (e1•eS2)-(e2•eL1) to (e2•eS1)(e2•eL1) conformational change] proceeds more rapidly. Note that the frontmost dimer can undergo sugar binding induced conformational changes while the L1 liganded dimer is locked in a dead-end (e2•eL1) state. Introduction of higher CCB levels fills both rear and front dimers with L1 to form the catalytically inactive complex (eL1•e2)(e2•eL1). ATP modulates ligand binding by increasing the affinity of the unliganded carrier for CCB or for S2 and by increasing the affinities of the S2 complexed carrier [e.g., (e1•eS2)(e1•e2)] for L1 and of the L1 complexed carrier [e.g., (eL1•e2)(e1•e2)] for S2 (shown by ATP → +). ATP also reduces the rate of S2 translocation (shown by ATP → −).

of cis and trans e2 sites for maltose is high and that 3MG transport through cis and trans e2 sites is slow. When subsaturating maltose (a nontransportable import site ligand) is introduced, occupancy of a high-affinity e2 subunit of either dimer (the liganded dimer is now defined as the cis dimer) (1) sterically blocks further conformational changes within both subunits of the cis dimer but enhances 3MG translocation through the e2 subunit of the unliganded (trans) dimer, (2) reduces the affinity of the trans e2 subunit for 3MG, and (3) increases the affinity of the trans e1 subunit for CCB. Occupancy of cis and trans e2 subunits by extracellular maltose (1) blocks e1 ↔ e2 conformational changes within all subunits of cis and trans dimers, thereby inhibiting 3MG transport, and (2) introduces negative cooperativity between maltose and CCB binding sites. This hypothesis explains why progressively increasing extracellular maltose stimulates and then inhibits 3MG uptake (*16*) and CCB binding (*16*) to red cell GluT1. An interesting tenet of this hypothesis is the requirement that cis and trans dimers may function independently of one another.

This hypothesis requires only minor adjustment to account for the effects of CCB on 3MG transport reported here. As with extracellular maltose occupancy of a high-affinity e2 subunit, CCB occupancy of a high-affinity e1 subunit blocks further conformational changes within the cis dimer but enhances 3MG translocation through the e2 subunit of the

unliganded trans dimer and increases the affinity of the e1 subunit of the unliganded trans dimer for CCB by 3-fold. Occupancy of cis and trans e1 subunits by CCB blocks conformational changes within all subunits, thereby arresting 3MG transport, and introduces negative cooperativity between maltose and CCB binding sites. This hypothesis explains why progressively increasing CCB stimulates and then inhibits 3MG uptake by red cell GluT1. In the absence of ATP, the affinities of cis and trans e1 sites for CCB are reduced 2-fold, the affinities of cis and trans e2 sites for 3MG are reduced by 10−20-fold, and translocation through e2 subunits is increased 8-fold. Subsequent occupancy of a cis e1 site by CCB increases the affinity of the trans e1 site for CCB by some 20-fold and increases 3MG translocation through the e2 subunit of the unliganded trans dimer by 2-fold. This hypothesis explains why ATP depletion increases red blood cell net 3MG uptake capacity (*79*; V_{max} is increased), why 3MG uptake at subsaturating [3MG] is inhibited by ATP depletion (*79*; V_{max}/K_m is decreased), and why CCB binding shows increased cooperativity in the absence of ATP.

APPENDIX

Kinetics. Consisting of 2 GluT1 dimers in which intradimer subunit interactions prevent subunits from adopting identical conformational states, each transporter exposes two import and two export sites at any instant (see Figure 7). For example, unoccupied carrier could present as (e1·e2)(e1·e2), as (e1·e2)(e2·e1), as (e2·e1)(e1·e2), or as (e2·e1)(e2·e1), where parentheses demark each dimer and e1 and e2 indicate the conformational states presented by individual subunits within the dimer. The implication is that cis and trans dimers are associated but are not linked to one another in an obligatory manner. In the absence or presence of the e1 ligand CCB (here denoted as L), four general forms of extracellular substrate (sugar, S) liganded carrier are capable of sugar uptake. These are carriers with one bound sugar but lacking CCB [e.g., (e1·eS2)(e1·e2)], carriers with two bound sugars but lacking CCB [e.g., (e1·eS2)(e1·eS2)], carriers with one bound sugar and one bound CCB [e.g., (e1·eS2)(eL1·e2); note the cis dimer (eL1·eS2) in the (eL1·eS2)(e1·e2) complex is inhibited, i.e., only one-half of all possible forms of S·e·L are functional], and carriers with two bound sugars but one CCB [e.g., (eL1·eS2)(e1·eS2); note the dimer containing cis sugar and CCB (eL1·eS2) is unable to catalyze sugar uptake]. Solving for sugar transport using the rapid equilibrium approach requires a stochastic approach in which one includes the number of possible forms of each carrier species (e.g., four ways to make unoccupied carrier), the number of transport competent forms, and the number of substrates translocated through each form [e.g., (e1·eS2)-(e1·eS2) translocates two sugar molecules whereas (eL1·eS2)(e1·eS2) translocates only one]. With these considerations in mind, a rapid equilibrium expression for GluT1-mediated sugar transport may be obtained as

$$v = \frac{V_{m(app)}S}{K_{m(app)} + S} \tag{1}$$

where S is the concentration of extracellular transportable sugar and

$$V_{m(app)} = \frac{8\left\{v_1 + v_2\frac{S}{\beta K} + v_3\frac{LS}{\beta K K_L} + v_4\frac{L}{\gamma K_L}\right\}}{8 + \frac{4S}{\beta K} + \frac{16L}{\gamma K_L} + \frac{8SL}{\beta\pi K K_L} + \frac{8LL}{\alpha\delta K_L^2} + \frac{4SLL}{\beta\pi\theta K K_L^2}} \tag{2}$$

and

$$K_{m(app)} = \frac{K\left(4 + \frac{L}{K_L}\left\{8 + \frac{4L}{\alpha K_L}\right\}\right)}{8 + \frac{4S}{\beta K} + \frac{16L}{\gamma K_L} + \frac{8SL}{\beta\pi K K_L} + \frac{8LL}{\alpha\delta K_L^2} + \frac{4SLL}{\beta\pi\theta K K_L^2}} \tag{3}$$

and the pseudo-first-order rate constant, τ, for sugar uptake at subsaturating S is given by

$$\tau = \frac{V_{m(app)}}{K_{m(app)}} = \frac{8\left\{v_1 + v_2\frac{S}{\beta K} + v_3\frac{LS}{\beta K K_L} + v_4\frac{L}{\gamma K_L}\right\}}{K\left(4 + \frac{L}{K_L}\left\{8 + \frac{4L}{\alpha K_L}\right\}\right)} \tag{4}$$

where L is the concentration of e1 ligand, K_L is the dissociation constant for L binding to e1, K is the dissociation constant for S binding to e2 in unliganded carrier, and v_1, v_2, v_3, and v_4 are the products {[GluT1]$_{total}$. translocation rate constant} for sugar uptake via carrier with only one bound sugar, two bound sugars, two bound sugars plus L, and one bound sugar plus L, respectively. α, β, δ, γ, π, and θ are cooperativity factors describing respectively how L binding to one dimer affects K_L for L bindng to the second dimer, how S binding to one e2 subunit affects K for S bindng to the remaining e2 site, how L binding to both dimers affects K for S binding to the cis or trans e2 subunit, how L binding to one dimer affects K for S binding to the cis or trans e2 subunit, how occupancy of the carrier by two S molecules affects K_L for L binding to either of the remaining e1 sites, and how occupancy of the carrier by S and by L affects the K_L for L binding to the remaining e1 site. If ligand binding to any given e1 subunit influences S binding to the cis e2 subunit (i.e., to the same dimer) differently than it does S binding to the trans e2 subunit (i.e., to the opposite, unliganded dimer), the denominators of eqs 2 and 3 are expanded to yield

$$\text{denom} = 8 + \frac{4S}{\beta K} + \frac{8L}{\gamma K_L} + \frac{8L}{\gamma' K_L} + \frac{8SL}{\beta\pi K K_L} + \frac{8LL}{\alpha\delta K_L^2} + \frac{4SLL}{\beta\pi\theta K K_L^2}$$

where γ' is the factor by which L binding affects K for S binding to a cis uptake binding site and γ is the factor by which L binding affects K for S binding to a trans uptake binding site. Only the trans sugar can be transported; the dimer containing cis L and cis S is inactive. The numerators to eqs 2 and 4 and the denominator to eq 4 are unaffected. Transport measurements do not, therefore, permit distinction between γ and γ'. This will require binding studies with

extracellular sugar and e1 ligand (e.g., see refs *10* and *11*). At subsaturating S, the rate of sugar uptake, v, is given by $v = \tau S$.

e1 ligand binding (L_b) to the transporter in the absence of S or ATP may be described by

$$L_b = \frac{B_{m(app)}L}{K_{d(app)} + L} + \chi L \quad (5)$$

where χ is a constant describing nonspecific L binding and

$$B_{max} = [\mathrm{GluT1}]\left\{\frac{4 + \frac{4L}{\alpha K_L}}{4 + \frac{2L}{\alpha K_L}}\right\} \quad (6)$$

and

$$K_{d(app)} = \frac{K_L}{2 + 2\frac{L}{\alpha K_L}} \quad (7)$$

The effects of ATP (N) on L binding were simulated by assuming that each subunit (GluT1 protein) is a functional ATP binding protein and allowing for cooperativity in ATP binding and also in S and N or S and L binding. This amplifies the complexity of the analysis considerably since there are now many more forms of N-complexed carrier with which S and/or L may interact. Binding of L in the presence of ATP (N) but in the absence of S is given by

$$L_b = L[\mathrm{GluTl}](\alpha K_L + L)/\left[L^2 + K_L\alpha\left\{2L + \frac{\varpi K_L(N^4 + 4\epsilon\varphi\sigma K_N^3 N + 6\epsilon\sigma K_N^2 N^2 + 4\sigma K_N N^3 + \epsilon\varphi\sigma K_N^4)}{N^4 + 4\epsilon\varphi\sigma K_N^3 N + 6\epsilon\sigma K_N^2 N^2 + 4\sigma K_N N^3 + \epsilon\varphi\varpi\sigma K_N^4}\right\}\right] \quad (8)$$

where N = [ATP], K_N is the dissociation constant for ATP binding to any available subunit of an ATP-free GluT1 tetramer, and α, ϵ, φ, σ, and ω are cooperativity factors describing respectively how L binding to one dimer affects K_L for L binding to the second dimer, how N binding to one subunit affects N binding to the next subunit, how N binding to two subunits affects N binding to the third subunit, how N binding to three subunits affects N binding to the remaining subunit, and how N binding to one subunit affects L binding to an available e1 subunit and vice versa.

ATP binding (N_b) in the absence of S but in the presence of L is described by

$$N_b = \frac{B_{m(app)}N}{K_{d(app)} + N} \quad (9)$$

where

$$B_{m(app)} = [\mathrm{GluTl}]\{N^3 + \epsilon\varphi\sigma K_N^3 + 3\sigma K_N N(\epsilon K_N + N)\} \times \{L^2 + \alpha K_L(2L + \varpi K_L)\}/[L\{2\alpha K_L + L\}\{N^3 + 2\sigma K_N(2N^2 + \epsilon K_N\{2\varphi K N + 3N\})\}] \quad (10)$$

and

$$K_{d(app)} = [\epsilon\varphi\varpi\sigma K_N^4 L^2 + \alpha\varpi K_L\{K_L N^4 + \sigma K_N(4K_L N^3 + \epsilon K_N\{6K_L N^2 + \varphi K_N(K_L K_N + 2K_N L + 4K_L N)\})\}]/[L\{2\alpha K_L + L\}\{N^3 + 2\sigma K_N(2N^2 + \epsilon K_N\{2\varphi K_N + 3N\})\}] \quad (11)$$

REFERENCES

1. Widdas, W. F. (1952) Inability of diffusion to account for placental glucose transfer in the sheep and consideration of the kinetics of a possible carrier transfer, *J. Physiol. (London) 118*, 23−39.
2. Lieb, W. R., and Stein, W. D. (1974) Testing and characterizing the simple carrier, *Biochim. Biophys. Acta 373*, 178−196.
3. Gunter, T. E., Wingrove, D. E., Banerjee, S., and Gunter, K. K. (1988) Mechanisms of mitochondrial calcium transport, *Adv. Exp. Med. Biol. 232*, 1−14.
4. Restrepo, D., Kozody, D. J., Spinelli, L. J., and Knauf, P. A. (1989) Cl−Cl exchange in promyelocytic HL-60 cells follows simultaneous rather than ping-pong kinetics, *Am. J. Physiol. 257*, C520−C527.
5. Palmieri, F., Indiveri, C., Bisaccia, F., and Kramer, R. (1993) Functional properties of purified and reconstituted mitochondrial metabolite carriers, *J. Bioenerg. Biomembr. 25*, 525−535.
6. Pos, K. M., and Dimroth, P. (1996) Functional properties of the purified Na(+)-dependent citrate carrier of Klebsiella pneumoniae: evidence for asymmetric orientation of the carrier protein in proteoliposomes, *Biochemistry 35*, 1018−1026.
7. Wingrove, D. E., and Gunter, T. E. (1986) Kinetics of mitochondrial calcium transport. II. A kinetic description of the sodium-dependent calcium efflux mechanism of liver mitochondria and inhibition by ruthenium red and by tetraphenylphosphonium, *J. Biol. Chem. 261*, 15166−15171.
8. Baker, G. F., and Naftalin, R. J. (1979) Evidence of multiple operational affinities for D-glucose inside the human erythrocyte membrane, *Biochim. Biophys. Acta 550*, 474−484.
9. Carruthers, A., and Helgerson, A. L. (1991) Inhibitions of sugar transport produced by ligands binding at opposite sides of the membrane. Evidence for simultaneous occupation of the carrier by maltose and cytochalasin B, *Biochemistry 30*, 3907−3915.
10. Helgerson, A. L., and Carruthers, A. (1987) Equilibrium ligand binding to the human erythrocyte sugar transporter. Evidence for two sugar-binding sites per carrier, *J. Biol. Chem. 262*, 5464−5475.
11. Sultzman, L. A., and Carruthers, A. (1999) Stop-flow analysis of cooperative interactions between GLUT1 sugar import and export sites, *Biochemistry 38*, 6640−6650.
12. Henderson, P. J., and Maiden, M. C. (1990) Homologous sugar transport proteins in *Escherichia coli* and their relatives in both prokaryotes and eukaryotes (review), *Philos. Trans. R. Soc. London, Ser. B: Biol. Sci. 326*, 391−410.
13. Paulsen, I. T., Sliwinski, M. K., and Saier, M. H., Jr. (1998) Microbial genome analyses: global comparisons of transport capabilities based on phylogenies, bioenergetics and substrate specificities, *J. Mol. Biol. 277*, 573−592.
14. Paulsen, I. T., Sliwinski, M. K., Nelissen, B., Goffeau, A., and Saier, M. H., Jr. (1998) Unified inventory of established and putative transporters encoded within the complete genome of *Saccharomyces cerevisiae*, *FEBS Lett. 430*, 116−125.
15. Mueckler, M. (1994) Facilitative glucose transporters, *Eur. J. Biochem. 219*, 713−725.
16. Hamill, S., Cloherty, E. K., and Carruthers, A. (1999) The human erythrocyte sugar transporter presents two sugar import sites, *Biochemistry 38*, 16974−16983.
17. Steck, T. L., and Yu, J. (1973) Selective solubilization of proteins from red blood cell membranes by protein perturbants, *J. Supramol. Struct. 1*, 220−232.
18. Baldwin, S. A., Baldwin, J. M., and Lienhard, G. E. (1982) The monosaccharide transporter of the human erythrocyte. Characterization of an improved preparation, *Biochemistry 21*, 3836−3842.

19. Hebert, D. N., and Carruthers, A. (1992) Glucose transporter oligomeric structure determines transporter function. Reversible redox-dependent interconversions of tetrameric and dimeric GLUT1, *J. Biol. Chem. 267*, 23829−23838.
20. Laemmli, U. K. (1970) *Nature 270*, 680−685.
21. Cloherty, E. K., Heard, K. S., and Carruthers, A. (1996) Human erythrocyte sugar transport is incompatible with available carrier models, *Biochemistry 35*, 10411−10421.
22. Levine, K. B., Cloherty, E. K., Fidyk, N. J., and Carruthers, A. (1998) Structural and physiologic determinants of human erythrocyte sugar transport regulation by adenosine triphosphate, *Biochemistry 37*, 12221−12232.
23. Segel, I. H. (1975) in *Enzyme Kinetics*, pp 161−162, Wiley, New York.
24. Sogin, D. C., and Hinkle, P. C. (1980) Binding of cytochalasin B to human erythrocyte glucose transport, *Biochemistry 19*, 5417−5420.
25. Deziel, M., Pegg, W., Mack, E., Rothstein, A., and Klip, A. (1984) Labeling of the human erythrocyte glucose transporter with ^{3}H-labeled cytochalasin B occurs via protein photoactivation, *Biochim. Biophys. Acta 772*, 403−406.
26. Hebert, D. N., and Carruthers, A. (1986) Direct evidence for ATP modulation of sugar transport in human erythrocyte ghosts, *J. Biol. Chem. 261*, 10093−10099.
27. Carruthers, A., and Helgerson, A. L. (1989) The human erythrocyte sugar transporter is also a nucleotide binding protein, *Biochemistry 28*, 8337−8346.
28. Hebert, D. N., and Carruthers, A. (1991) Cholate-solubilized erythrocyte glucose transporters exist as a mixture of homodimers and homotetramers, *Biochemistry 30*, 4654−4658.
29. Heard, K. S., Fidyk, N., and Carruthers, A. (2000) ATP-dependent substrate occlusion by the human erythrocyte sugar transporter, *Biochemistry 39*, 3005−3014.
30. Zottola, R. J., Cloherty, E. K., Coderre, P. E., Hansen, A., Hebert, D. N., and Carruthers, A. (1995) Glucose transporter function is controlled by transporter oligomeric structure. A single, intramolecular disulfide promotes GLUT1 tetramerization, *Biochemistry 34*, 9734−9747.
31. Coderre, P. E., Cloherty, E. K., Zottola, R. J., and Carruthers, A. (1995) Rapid substrate translocation by the multi-subunit, erythroid glucose transporter requires subunit associations but not cooperative ligand binding, *Biochemistry 34*, 9762−9773.
32. Shanahan, M. F. (1982) Cytochalasin B: a natural photoaffinity ligand for labeling the human erythrocyte glucose transporter, *J. Biol. Chem. 257*, 7190−7293.
33. Basketter, D. A., and Widdas, W. F. (1978) Asymmetry of the hexose transfer system in human erythrocytes. Comparison of the effects of cytochalasin B, phloretin and maltose as competitive inhibitors, *J. Physiol. (London) 278*, 389−401.
34. Cloherty, E. K., Diamond, D. L., Heard, K. S., and Carruthers, A. (1996) Regulation of GLUT1-mediated sugar transport by an antiport/uniport switch mechanism, *Biochemistry 35*, 13231−13239.
35. Wardinski, B. E., Shanahan, M. F., and Ruoho, A. (1987) Derivatization of the human erythrocyte glucose transporter using a novel forskolin photoaffinity label, *J. Biol. Chem. 262*, 17683−17689.
36. Segel, I. H. (1975) in *Enzyme Kinetics*, pp 100−125, Wiley, New York.
37. Carter-Su, C., Pessin, J. E., Mova, R., Gitomer, W., and Czech, M. P. (1982) Photoaffinity labeling of the human erythrocyte D-glucose transporter, *J. Biol. Chem. 257*, 5419−5425.
38. Jung, C. Y., and Rampal, A. L. (1977) Cytochalasin B binding sites and glucose transport carrier in human erythrocyte ghosts, *J. Biol. Chem. 252*, 5456−5463.
39. Heard, K. S., Diguette, M., Heard, A. C., and Carruthers, A. (1998) Membrane-bound glyceraldehyde-3-phosphate dehydrogenase and multiphasic erythrocyte sugar transport, *Exp. Physiol. 83*, 195−201.
40. Shanahan, M. F., Morris, D. P., and Edwards, B. M. (1987) [^{3}H]-forskolin. Direct photoaffinity labeling of the erythrocyte D-glucose transporter, *J. Biol. Chem. 262*, 5978−5984.
41. Carruthers, A., and Melchior, D. L. (1983) Asymmetric or symmetric? Cytosolic modulation of human erythrocyte hexose transfer, *Biochim. Biophys. Acta 728*, 254−266.
42. Carruthers, A. (1991) Mechanisms for the facilitated diffusion of substrates across cell membranes, *Biochemistry 30*, 3898−3906.
43. Carruthers, A., and Melchior, D. L. (1984) Human erythrocyte hexose transporter activity is governed by bilayer lipid composition in reconstituted vesicles, *Biochemistry 23*, 6901−6911.
44. Haneskog, L., Andersson, L., Brekkan, E., Englund, A. K., Kameyama, K., Liljas, L., Greijer, E., Fischbarg, J., and Lundahl, P. (1996) Monomeric human red cell glucose transporter (Glut1) in nonionic detergent solution and a semi-elliptical torus model for detergent binding to membrane proteins, *Biochim. Biophys. Acta 1282*, 39−47.
45. Sogin, D. C., and Hinkle, P. C. (1978) Characterization of the glucose transporter from human erythrocytes, *J. Supramol. Struct. 8*, 447−453.
46. Zoccoli, M. A., Baldwin, S. A., and Lienhard, G. E. (1978) The monosaccharide transport system of the human erythrocyte. Solubilization and characterization on the basis of cytochalasin B binding, *J. Biol. Chem. 253*, 6923−6930.
47. Jung, C. Y., Hsu, T. L., Cha, J. S., and Haas, M. N. (1980) Glucose transport carrier of human erythrocytes. Radiation-target size of glucose-sensitive cytochalasin B binding protein, *J. Biol. Chem. 225*, 361−364.
48. Cloherty, E. K., Hamill, S., Levine, K., and Carruthers, A. (2001) Sugar Transporter Regulation by ATP and quaternary structure, *Blood Cells, Mol. Dis. 27*, 102−107.
49. Casey, J. R., and Reithmeier, R. A. (1991) Analysis of the oligomeric state of Band 3, the anion transport protein of the human erythrocyte membrane, by size exclusion high performance liquid chromatography. Oligomeric stability and origin of heterogeneity, *J. Biol. Chem. 266*, 15726−15737.
50. Kelleher, D. J., and Gilmore, R. (1994) The *Saccharomyces cerevisiae* oligosaccharyltransferase is a protein complex composed of Wbp1p, Swp1p, and four additional polypeptides, *J. Biol. Chem. 269*, 12908−12917.
51. Hanein, D., Matlack, K. E., Jungnickel, B., Plath, K., Kalies, K. U., Miller, K. R., Rapoport, T. A., and Akey, C. W. (1996) Oligomeric rings of the Sec61p complex induced by ligands required for protein translocation (see comments), *Cell 87*, 721−732.
52. Rampal, A. L., Jung, E. K., Chin, J. J., Deziel, M. R., Pinkofsky, H. B., and Jung, C. Y. (1986) Further characterization and chemical purity assessment of the human erythrocyte glucose transporter preparation, *Biochim. Biophys. Acta 859*, 135−142.
53. Cairns, M. T., Alvarez, J., Panico, M., Gibbs, A. F., Morris, H. R., Chapman, D., and Baldwin, S. A. (1987) Investigation of the structure and function of the human erythrocyte glucose transporter by proteolytic dissection, *Biochim. Biophys. Acta 905*, 295−310.
54. Casey, J. R., and Reithmeier, R. A. (1993) Detergent interaction with band 3, a model polytopic membrane protein, *Biochemistry 32*, 1172−1179.
55. Walz, T., Smith, B. L., Agre, P., and Engel, A. (1994) The three-dimensional structure of human erythrocyte aquaporin CHIP, *EMBO J. 13*, 2985−2993.
56. Fu, D., Libson, A., Miercke, L. J., Weitzman, C., Nollert, P., Krucinski, J., and Stroud, R. M. (2000) Structure of a glycerol-conducting channel and the basis for its selectivity, *Science 290*, 481−486.
57. Moore-Hoon, M. L., and Turner, R. J. (2000) The structural unit of the secretory Na^+-K^+-$2Cl^-$ cotransporter (NKCCl) is a homodimer, *Biochemistry 39*, 3718−3724.
58. McMurry, L. M., and Levy, S. B. (1995) The NH_2 terminal half of the Tn10-specified tetracycline efflux protein tetA contains a dimerization domain, *J. Biol. Chem. 270*, 22752−22757.
59. Yin, C. C., Aldema-Ramos, M. L., Borges-Walmsley, M. I., Taylor, R. W., Walmsley, A. R., Levy, S. B., and Bullough, P. A. (2000) The quaternary molecular structure of TetA, a

secondary tetracycline transporter from *Escherichia coli*, *Mol. Microbiol. 38*, 482−492.
60. Fafournoux, P., Noël, J., and Pouysségur, J. (1994) Evidence that the Na^+H^+ exchanger isoforms NHE1 and NHE3 exist as stable dimers in membranes with a high specificity for homodimers, *J. Biol. Chem. 269*, 2589−2596.
61. Williams, K. A. (2000) Three-dimensional structure of the ion-coupled transport protein NhaA, *Nature 403*, 112−115.
62. Gerchman, Y., Rimon, A., Venturi, M., and Padan, E. (2001) Oligomerization of NhaA, the Na+/H+ antiporter of *Escherichia coli* in the membrane and its functional and structural consequences, *Biochemistry 40*, 3403−3412.
63. Veenhoff, L. M., Heuberger, E. H., and Poolman, B. (2001) The lactose transport protein is a cooperative dimer with two sugar translocation pathways, *EMBO J. 20*, 3056−3062.
64. Mueckler, M., and Makepeace, C. (1999) Transmembrane segment 5 of the Glut1 glucose transporter is an amphipathic helix that forms part of the sugar permeation pathway, *J. Biol. Chem. 274*, 10923−10926.
65. Olsowski, A., Monden, I., and Keller, K. (1998) Cysteine-scanning mutagenesis of flanking regions at the boundary between external loop I or IV and transmembrane segment II or VII in the GLUT1 glucose transporter, *Biochemistry 37*, 10738−10745.
66. Wellner, M., Monden, I., and Keller, K. (1995) From triple cysteine mutants to the cysteine-less glucose transporter GLUT1: a functional analysis, *FEBS Lett. 370*, 19−22.
67. Wellner, M., Monden, I., and Keller, K. (1992) The differential role of Cys-421 and Cys-429 of the Glut1 glucose transporter in transport inhibition by *p*-chloromercuribenzenesulfonic acid (pCMBS) or cytochalasin B (CB), *FEBS Lett. 309*, 293−296.
68. Mueckler, M., and Makepeace, C. (1997) Identification of an amino acid residue that lies between the exofacial vestibule and exofacial substrate-binding site of the Glut1 sugar permeation pathway, *J. Biol. Chem. 272*, 30141−30146.
69. Due, A. D., Cook, J. A., Fletcher, S. J., Qu, Z. C., Powers, A. C., and May, J. M. (1995) A "cysteineless" GLUT1 glucose transporter has normal function when expressed in Xenopus oocytes, *Biochem. Biophys. Res. Commun. 208*, 590−596.
70. Wellner, M., Monden, I., and Keller, K. (1994) The role of cysteine residues in glucose-transporter-GLUT1-mediated transport and transport inhibition, *Biochem. J. 299*, 813−817.
71. Harrison, S. A., Buxton, J. M., and Czech, M. P. (1991) Suppressed intrinsic catalytic activity of GLUT1 glucose transporters in insulin-sensitive 3T3-L1 adipocytes, *Proc. Natl. Acad. Sci. U.S.A. 88*, 7839−7843.
72. Harrison, S. A., Buxton, J. M., Helgerson, A. L., MacDonald, R. G., Chlapowski, F. J., Carruthers, A., and Czech, M. P. (1990) Insulin action on activity and cell surface disposition of human HepG2 glucose transporters expressed in Chinese hamster ovary cells, *J. Biol. Chem. 265*, 5793−5801.
73. Levine, K. B., Hamill, S., Cloherty, E. K., and Carruthers, A. (2001) Alanine Scanning Mutagenesis of the Human Erythrocyte Glucose Transporter Putative ATP Binding Domain, *Blood Cells, Mol. Dis. 27*, 139−142.
74. Wheeler, T. J., and Hinkle, P. C. (1981) Kinetic properties of the reconstituted glucose transporter from human erythrocytes, *J. Biol. Chem. 256*, 8907−8914.
75. Appleman, J. R., and Lienhard, G. E. (1989) Kinetics of the purified glucose transporter. Direct measurement of the rates of interconversion of transporter conformers, *Biochemistry 28*, 8221−8227.
76. Lowe, A. G., and Walmsley, A. R. (1986) The kinetics of glucose transport in human red blood cells, *Biochim. Biophys. Acta 857*, 146−154.
77. Stein, W. D. (1986) *Transport and diffusion across cell membranes*, Academic Press, New York.
78. Carruthers, A., and Zottola, R. J. (1996) in *Handbook of Biological Physics. Transport Processes in Eukaryotic and Prokaryotic Organisms* (Konings, W. N., H. R. K. J. S. L., Eds.) pp 311−342, Elsevier, New York.
79. Helgerson, A. L., Hebert, D. N., Naderi, S., and Carruthers, A. (1989) Characterization of two independent modes of action of ATP on human erythrocyte sugar transport, *Biochemistry 28*, 6410−6417.

BI015586W